RESEARCH ARTICLE | MARCH 01 2020

Excess entropy scaling for soft particle glasses

Special Collection: Physics of Dense Suspensions

Roger T. Bonnecaze ; Fardin Khabaz ; Lavanya Mohan ; Michel Cloitre

J. Rheol. 64, 423–431 (2020)
https://doi.org/10.1122/1.5133852
CHORUS

Excess entropy scaling for soft particle glasses

Roger T. Bonnecaze,[1,a)] Fardin Khabaz,[1] Lavanya Mohan,[1,b)] and Michel Cloitre[2]

[1]*McKetta Department of Chemical Engineering, The University of Texas at Austin, Austin, Texas 78712*
[2]*Molecular, Macromolecular Chemistry, and Materials, ESPCI Paris, CNRS, PSL University, 10 Rue Vauquelin, 75005 Paris, France*

(Received 27 October 2019; final revision received 18 January 2020; published 5 March 2020)

Abstract

The transport properties of soft particle glasses, such as dynamic viscosity, normal stress coefficients, and shear-induced diffusivity of its particles, are determined by the microstructure of the suspension under flow. A thermodynamic measure of the microstructure is the excess entropy, which we show here accurately correlates the transport properties of soft particle glasses onto master curves across a wide range of volume fractions, suspending fluid viscosities, particle moduli, and shear rates. The excess entropy for soft particle glasses is approximated with the two-body excess entropy computed from the pair distribution function extracted from dynamic simulations. The shear viscosity and normal stress functions diverge and the diffusivity vanishes at a critical excess entropy, corresponding to the yield stress of the suspension. An effective temperature is computed and is found to vary linearly with the shear stress and the elastic energy of the sheared soft particle glass. From this, an equation of state is derived relating the excess entropy to the shear stress. Consequently, three of the four transport properties are determined from the measurement of just one. Finally, a single master curve of particle diffusivity versus excess entropy is presented that unifies observations for both equilibrium and nonequilibrium suspensions. © *2020 The Society of Rheology.*
https://doi.org/10.1122/1.5133852

I. INTRODUCTION

In 1977, Rosenfeld proposed and showed for the first time that the diffusivity and viscosity of fluids composed of particles interacting with Lennard–Jones and short-ranged repulsive interparticle potentials are correlated onto a master curve as a function of the excess entropy of the system [1]. Separately, Dzugutov showed a similar correlation for liquid metals [2]. Many other studies have followed using excess entropy as a means to correlate the diffusivity and viscosity for a variety of atomic, molecular, and colloidal systems and interparticle potentials [3–17]. Truskett and co-workers have also shown how the correlation extends to particles in confined systems, thus connecting the properties in confinement to those in the bulk [8,18]. In all these studies, the systems were at equilibrium and there was no flow.

In Rosenfeld's and Dzugutov's original works, the normalized or so-called reduced diffusivity and viscosity were found to scale like $e^{\alpha S^E}$ and $e^{-\beta S^E}$, respectively, where S^E is the dimensionless excess entropy relative to that of an ideal gas on a per particle basis and normalized by the Boltzmann factor. Note that the excess entropy is negative. The constants α and β are positive, typically about equal and around 0.65–0.95. The normalization for the diffusivity and viscosity is based on the characteristic length and time scales for the systems of interest. While these scalings are observed for moderate values of the excess entropy, the diffusivity increases according to $-1/S^E$ at low values [10]. In this paper, we show that the diffusivity can also vanish as S^E approaches a value of the excess entropy S^E_y, corresponding to its value at the yield stress of the suspension. In general, if the normalized dynamic properties of a material at different temperatures and pressures are determined by S^E, it is said to obey the excess entropy scaling [4]. The success of this scaling was initially argued to be based on the excess entropy being a measure of the free volume available to the particles, which is the underlying microstructural determinant for the transport properties of the system [1,5,12].

The excess entropy scaling does not always work [4,19]. For example, systems of particles that interact with potentials with distinct directional bonding do not obey the excess entropy scaling. The exact requirement is that the interparticle potential be Euler homogeneous, i.e., $U(\lambda \mathbf{R}) = \lambda^{-n} U(\mathbf{R})$, where U is the potential energy for the system, $\mathbf{R}$ is the coordinates of the configuration, and λ is a scaling factor [4]. In practice, if this is approximately satisfied, the excess entropy scaling will collapse the dynamic properties of the system.

Here, we explore the effectiveness of using the excess entropy to correlate transport properties of athermal, jammed suspensions activated by shear, specifically soft particles glasses (SPGs). SPGs are concentrated suspensions of deformable particles such as microgels, droplets, and micelles. The volume concentration of these suspensions is well above random close packing for spheres. The dominant forces for these materials are repulsive elastic or Hertzian-like interparticle interactions, which are typically much larger than thermal forces. At rest, the suspension is in a trapped glassy state.

Note: This paper is part of the special issue on Physics of Dense Suspensions.
[a)]Author to whom correspondence should be addressed; electronic mail: rtb@che.utexas.edu
[b)]Present address: Exxon Mobil Upstream Research Company, 3120 Buffalo Speedway, Houston, TX 77098.

Under shear flow, the particles become mobile and can diffuse. The shear and normal stresses for SPGs follow a Herschel–Bulkley (HB) form [20–22]. All previous examples of the excess entropy scaling are for quiescent, thermally equilibrated systems, except for a few studies on the shear viscosity of attractive particles with significant thermal forces [23–25]. This paper aims to answer the following questions. Does the excess entropy correlation work for a nonequilibrium, athermal, shear activated system to correlate diffusivity and the shear and normal stress viscosities of SPGs? Can one construct a temperature and an equation of state for the SPGs connecting rheological properties to excess entropy? Finally, is there a universal scaling with excess entropy for diffusivity for colloidal systems regardless of whether they are thermally or shear activated?

II. SIMULATION METHODS

The details of the model and the simulation method have been presented in previous studies [20–22,26–28]. Here, we briefly summarize the essential features. Soft particle glasses are modeled as suspensions of 10^4 non-Brownian elastic particles in a solvent with a viscosity of η_s that are jammed at volume fractions larger than the random close packing of hard spheres. Suspensions with an average radius of unity scaled by the average radius R, polydispersity index of $\delta = 0.2$ [21,27], and volume fractions of $\phi = 0.7$, 0.75, 0.8, 0.85, and 0.9 are studied. At contact between particles α and β, they create a flat facet resulting in a deformation of $\varepsilon_{\alpha,\beta} = 0.5(R_\alpha + R_\beta - r_{\alpha\beta})/R_c$, where R_α and R_β are the radii of particle α and β, $r_{\alpha\beta}$ is the center-to-center distance, and R_c is the contact radius, which is given as $R_c = R_\alpha R_\beta/(R_\alpha + R_\beta)$.

The elastic repulsion force between particles α and β acts perpendicularly to the contacting facet (i.e., $\mathbf{n}_\perp$). It is given by the generalized Hertz law [20],

$$\mathbf{f}^e_{\alpha\beta} = \frac{4}{3} C E^* \varepsilon^n_{\alpha\beta} R_c^2 \mathbf{n}_\perp, \tag{1}$$

where E^* is the particle contact modulus: $E^* = E/2(1-\nu^2)$, with E being the Young modulus and $\nu = 0.5$ being the Poisson ratio. C and n are parameters, which depend on the degree of compression. For $\varepsilon < 0.1$, $n = 1.5$ and $C = 1$, for $0.1 \le \varepsilon < 0.2$, $n = 3$ and $C = 32$, and if $0.2 \le \varepsilon < 0.6$, $n = 5$ and $C = 790$ [20,29]. The elastohydrodynamic drag force, which is due to the existence of thin films of solvent between the flat facets of two particles in contact during the shear deformation [20], is parallel to the contacting facets and is given by

$$\mathbf{f}^{\mathrm{EHD}}_{\alpha\beta} = -(\eta_s C u_{\alpha\beta,||} E^* R_c^3)^{1/2} \varepsilon^{(2n+1)/4}_{\alpha\beta} \mathbf{n}_{||}, \tag{2}$$

where $u_{\alpha\beta,||}$ is the relative velocity component in the direction of parallel to the contacting facets (i.e., $\mathbf{n}_{||}$). The fluid inertia is neglected, and the forces are assumed to be pairwise additive. The velocity field due to the motion of the solvent is given as $\mathbf{u}^\infty_\alpha = \frac{\dot\gamma \eta_s}{E^*} y \mathbf{e}_x$, where $\mathbf{e}_x$ is the basis vector in the x-direction. The resulting equation of motion is made dimensionless by scaling lengths, time, and velocity by R, $\dot\gamma^{-1}$, and $\dot\gamma R$ respectively, leading to [20,28]

$$\frac{d\tilde{\mathbf{x}}_\alpha}{d\tilde t} = \tilde{\mathbf{u}}^\infty_\alpha + \frac{M}{\tilde R_\alpha}\left[\frac{4}{3} C \tilde{\dot\gamma}^{-1} \sum_\beta \varepsilon^n_{\alpha\beta} \tilde R_c^2 \mathbf{n}_\perp - \tilde{\dot\gamma}^{-1/2} \sum_\beta (C \tilde u_{\alpha\beta,||} \tilde R_c^3)^{1/2} \varepsilon^{(2n+1)/4}_{\alpha\beta} \mathbf{n}_{||}\right], \tag{3}$$

where the tilde quantities are dimensionless variables. M is the mobility function which is that of a particle corrected by a factor $f(\phi)$ that accounts for its reduction at high volume fraction, namely, $M = f(\phi)/6\pi$; $f(\phi)$ is set to 0.01 in the simulations. $\mathbf{x}_\alpha$ is the position of the particle α. The form of this equation shows that the dynamics is characterized by the dimensionless shear rate $\tilde{\dot\gamma} = \dot\gamma \eta_s/E^*$, which represents the ratio of viscous to elastic forces, and the overlap deformation that depends on the volume fraction. The Lees–Edwards [30] boundary conditions are then used in the LAMMPS package [31] in order to impart the desired shear rate to the simulation box.

Given the position of the particles at any instant in time, the stress, elastic energy, and entropy of the SPG under shear can be computed. The stress tensor of the suspensions is determined using the Kirkwood formula [32],

$$\boldsymbol{\sigma} = \frac{1}{V} \sum_\beta^N \sum_{\alpha>\beta}^N \mathbf{f}_{\alpha\beta}(\mathbf{x}_\alpha - \mathbf{x}_\beta), \tag{4}$$

where V is the volume of the system and $\mathbf{f}_{\alpha\beta} = \mathbf{f}^e_{\alpha\beta} + \mathbf{f}^{EHD}_{\alpha\beta}$ is the total force acting on particle α from particle β. The shear stress, σ_{xy}, and the first and second normal stress differences, $N_1 = \sigma_{xx} - \sigma_{yy}$ and $N_2 = \sigma_{yy} - \sigma_{zz}$, are computed from the appropriate components of the stress tensor. The dimensionless average elastic energy per volume of the SPGs is determined from the pairwise interaction energy between particles according to

$$U = \frac{8}{3N} \sum_{\alpha=1}^N \sum_{\beta>\alpha}^N \frac{C \varepsilon^{n+1}_{\alpha\beta} R_c^3}{(n+1)}, \tag{5}$$

where the C and n parameters are those used in the force law in Eq. (1). The elastic energy here is nondimensionalized by $E^* R^3$.

The excess entropy of the SPGs is approximated by determining the two-body contribution to the entropy as follows [3]:

$$S^E \cong S_2 = -\frac{1}{2}\rho \int [g(\mathbf{r}) \ln(g(\mathbf{r})) - g(\mathbf{r}) + 1] d\mathbf{r}, \tag{6}$$

where S^E is the dimensionless excess entropy per particle, $g(\mathbf{r})$ is the pair distribution function between the particles

that is determined in a steady-state flow condition, and ρ is the number density of the SPGs. The excess entropy is nondimensionalized by the Boltzmann factor k_B. The temperature T is calculated from the derivative of the energy with respect to the excess entropy, i.e., $T = (dU/dS^E)_{N,V}$. The temperature reported here is nondimensionalized by E^*R^3/k_B. Equation (6) has been used successfully to compute the excess entropy for liquids. SPGs are certainly not typical liquids in that they are shear rather than thermally activated. That being said, they have a pair distribution functions that shows no long range order and approaches unity around three particle diameters from the reference particle, similar to other liquids [20,33].

The flow properties and microstructure of the suspensions were investigated over a broad range of shear rates ranging from $\tilde{\dot{\gamma}} = 10^{-9}$ to $\tilde{\dot{\gamma}} = 10^{-4}$. The simulations were performed for 100 strain units, and the stress tensor is calculated at regular strain intervals. The value of the time step was chosen such that it produced 10^7 steps per strain at each shear rate.

III. RESULTS

A. Overview of rheology and dynamics of SPGs

The steady-state dimensionless shear stress σ/E^* is plotted against the dimensionless shear rate $\dot{\gamma}\eta_s/E^*$ in Fig. 1(a). Suspensions show a yield behavior at very low shear rates, and then by increasing the shear rate, they start flowing. The magnitude of the yield stress σ_y/E^* increases with the volume fraction of suspensions. Similarly, the first and second normal stress differences (N_1/E^* and $-N_2/E^*$) are plotted as a function of the shear rate in Figs. 1(b) and 1(c) for SPGs with different volume fractions. At low shear rates, a similar yield behavior as seen in Fig. 1(a) is observed for normal stress differences in Figs. 1(b) and 1(c). This yield behavior is followed-up by the power-law increase of the shear stress at high shear rates (i.e., shear thinning regime). The shear rate is rescaled using the low-frequency modulus G_0 of these pastes, i.e., $\dot{\gamma}\eta_s/G_0$ [26,34]. The rescaled shear stress σ/σ_y collapses onto a master curve, and they follow the HB relationship with an exponent of 0.48 for the shear stress as seen in Fig. 1(d) [σ_y is obtained from fitting the individual shear stress data in Fig. 1(a) to the HB relationship]. The normalized stress differences also show a universal trend as a function of the shear rate $\dot{\gamma}\eta_s/G_0$ as seen in Figs. 1(e) and 1(f).

The shear-induced diffusion coefficient of the suspensions is determined from the diffusive part of the mean-squared displacement of the SPGs [22] at different shear rates to characterize the dynamics of SPGs. As seen in Fig. 2, the diffusion coefficient data collapse onto a master curve. At low shear rates, the rescaled diffusion coefficient $D\eta_s/G_0R^2$ follows a linear relationship as a function of the shear rate, while at high shear rates (where stress increases in a power-law fashion), we observe a power-law relationship between the $D\eta_s/G_0R^2$ and $\dot{\gamma}\eta_s/G_0$ with an exponent of 2/3. The crossover between the low and high shear regimes is determined from the intersection between the power-law behaviors at low and high shear rates, around $\dot{\gamma}\eta_S/G_0 \cong 5 \times 10^{-6}$, as noted by Khabaz *et al.* [22]. It is noteworthy that this value is the same as the one that marks the crossover between the low shear plateau and the power-law regime for the shear stress in Fig. 1(d).

The elastic energy U of the SPGs at different volume fractions is determined using Eq. (5) at different shear rates $\dot{\gamma}\eta_s/E^*$. As seen in Fig. 3(a), at low shear rates, the elastic energy shows a yield value, and then it increases in a power-law fashion according to the HB relationship [elastic energy

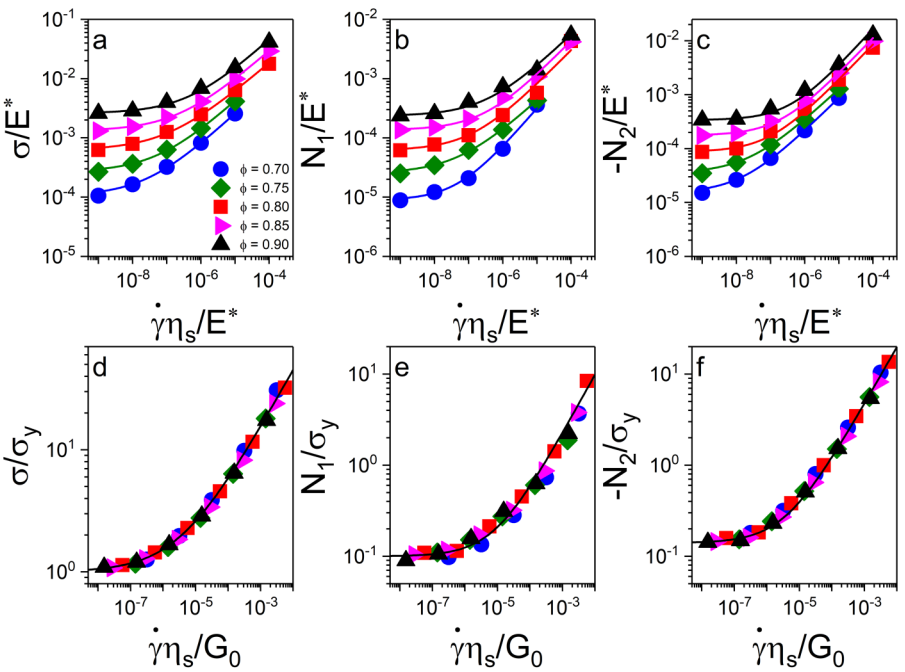

FIG. 1. (a) Shear stress σ/E^*, (b) first N_1/σ_y, and (c) second normal stress differences $-N_2/\sigma_y$ as a function of the shear rate $\dot{\gamma}\eta_s/E^*$. Rescaled (d) shear stress σ/σ_y, (e) first N_1/σ_y, and (f) second normal stress differences $-N_2/\sigma_y$ as a function of the rescaled shear rate $\dot{\gamma}\eta_s/G_0$. The lines in (d)–(f) are the best fits of the data to the HB equation: $\sigma/\sigma_y = 1 + 404(\dot{\gamma}\eta_s/G_0)^{0.48\pm0.02}$, $N_1/\sigma_y = 0.1 + 195(\dot{\gamma}\eta_s/G_0)^{0.65\pm0.02}$, and $-N_2/\sigma_y = 0.14 + 359(\dot{\gamma}\eta_s/G_0)^{0.63\pm0.02}$.

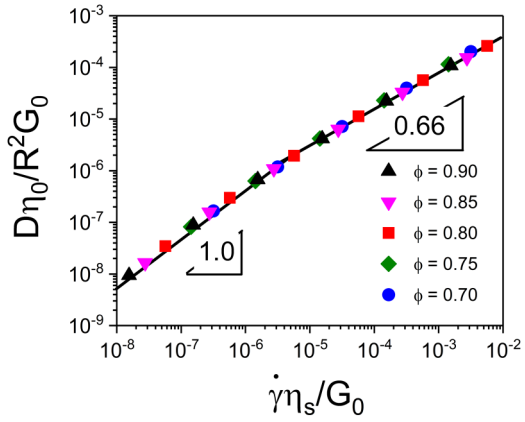

FIG. 2. The diffusion coefficient $D\eta_s/G_0R^2$ as a function of the rescaled shear rate $\dot{\gamma}\eta_s/G_0$.

data in each volume fraction are fitted to the HB relationship $U = U_y + k(\eta_s\dot{\gamma}/E^*)^n$ and the yield value of the elastic energy U_y is extracted]. The yield value of the elastic energy U_y increases with the volume fraction of suspensions. Using the rescaled shear rate $\dot{\gamma}\eta_s/G_0$, all elastic energy data collapse onto a master curve as demonstrated in Fig. 3(b).

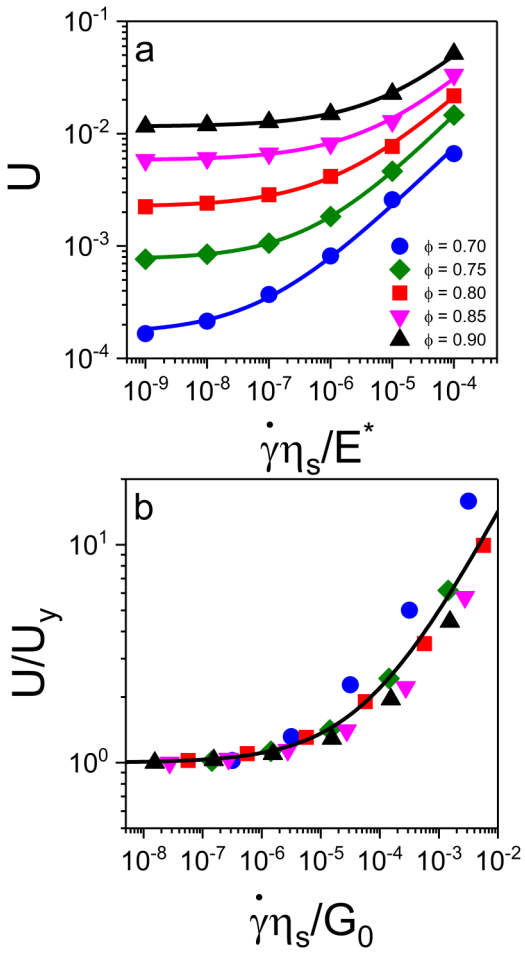

FIG. 3. (a) Elastic energy U as a function of shear rate $\dot{\gamma}\eta_s/E^*$ and (b) master curve of the rescaled elastic energy U/U_y as a function of the rescaled shear rate $\dot{\gamma}\eta_s/G_0$ for SPGs with different volume fractions. The solid lines in (a) show the HB equation fit to data given by $U = U_y + k(\eta_s\dot{\gamma}/E^*)^n$. The solid line in (b) shows the HB equation fit to data given by $U/U_y = 1 + 145(\eta_S\dot{\gamma}/G_0)^{0.52}$.

B. Excess entropy of SPGs and connection with macroscopic properties

The pair distribution function between the soft particles is computed and then used to calculate the excess entropy according to Eq. (6). The values of $-S^E$ are plotted against the shear rate for SPGs with different volume fractions in Fig. 4(a). At low shear rates, the values of $-S^E$ plateau around a value of 9.0. As the shear rate increases, the excess entropy increases (i.e., $-S^E$ becomes less negative) due to the effect of shear flow, and it decreases with the volume fraction in the shear thinning part of the flow curve. All excess entropy data collapse onto a master curve when plotted against the rescaled shear rate $\dot{\gamma}\eta_s/G_0$. The agreement is less good for $\phi = 0.7$ and the lowest shear rates. The poorer agreement here is unknown at this time. It may be that the two-body approximation to the excess entropy may be less accurate for these conditions. It is also possible that the excess entropy scaling fails under these conditions. It has been noted that systems that become nonergodic fail the entropy scaling and show lower than expected diffusivities compared to the ergodic systems where the scaling works [35].

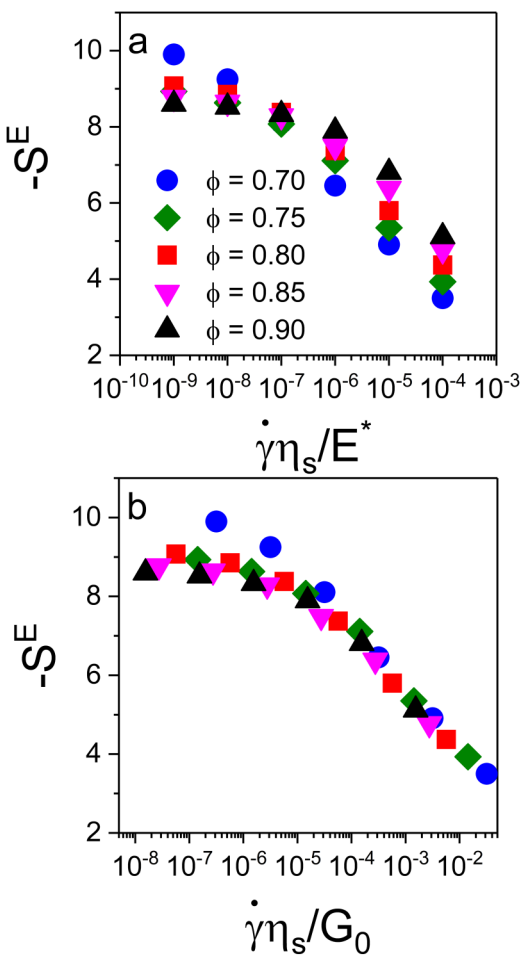

FIG. 4. (a) Excess entropy $-S^E$ as a function of shear rate $\dot{\gamma}\eta_s/E^*$ for SPGs with different volume fractions. (b) Master curve of $-S^E$ as a function of the rescaled shear rate $\dot{\gamma}\eta_s/G_0$.

Using the elastic energy and the excess entropy, we can define a "temperature" of the sheared suspension based on the thermodynamic relationship $T = (dU/dS^E)_{N,V}$. The values of the elastic energy U as a function of $-S^E$ are fitted to a power-law relationship, and then the temperature T is extracted (see Fig. S1 in supplementary material [37] for U versus $-S^E$). The values of the temperature T at different volume fractions and shear rates are shown in Fig. 5. The temperature T at low shear rates near the yield stress is constant for a given volume fraction and is denoted by T_y. As the shear rate increases, the temperature of the SPGs increases based on the HB relationship. Furthermore, the temperature increases with an increase in the volume fraction of the suspensions. Using the normalized values of the temperature with respect to the yield temperature (i.e., T/T_y) and the rescaled shear rate of $\dot{\gamma}\eta_s/G_0$, a master curve of the temperature is constructed in Fig. 5(b). As seen in the figure, the T/T_y values follow the HB equation with an exponent of 0.52. The transition temperature between the quasistatic and shear thinning regimes occurs at a shear rate of $\dot{\gamma}\eta_s/G_0 \cong 5 \times 10^{-6}$ in agreement with our previous findings for the flow curves and cage relaxation time in these jammed suspensions [22].

We relate the elastic energy U and shear stress σ/E^* to the temperature T in Figs. 6(a) and 6(b), respectively. As seen in Fig. 6(a), the elastic energy shows a universal behavior for all the SPGs with different volume fractions, and it increases linearly with the temperature as $U = (1.65 \pm 0.10)T$. The shear stress also exhibits a universal linear trend as a function of the temperature as $\sigma = (1.31 \pm 0.05)T$ as seen in Fig. 6(b). The linear relationships between energy, stress, and temperature of SPGs were anticipated in earlier studies [21,27,36]. Mohan and Bonnecaze [36] used energy as a surrogate for temperature in the expression $-U\nabla \ln g(\mathbf{r})$ for the effective nonequilibrium elastic force acting on a particle in a SPG, analogous to a Brownian force [36]. Suspensions of SPGs under sufficiently high shear will transition from a glass microstructure to a layered one at sufficiently high shear rates [21,27]. The transition is an activated process following an Arrhenius behavior if one uses stress rather than temperature [21].

In order to establish a connection between the dynamics of SPGs and the excess entropy, the rescaled diffusion coefficient values are plotted against $-S^E$ in Fig. 7(a). The diffusion coefficient increases with an increase in the excess

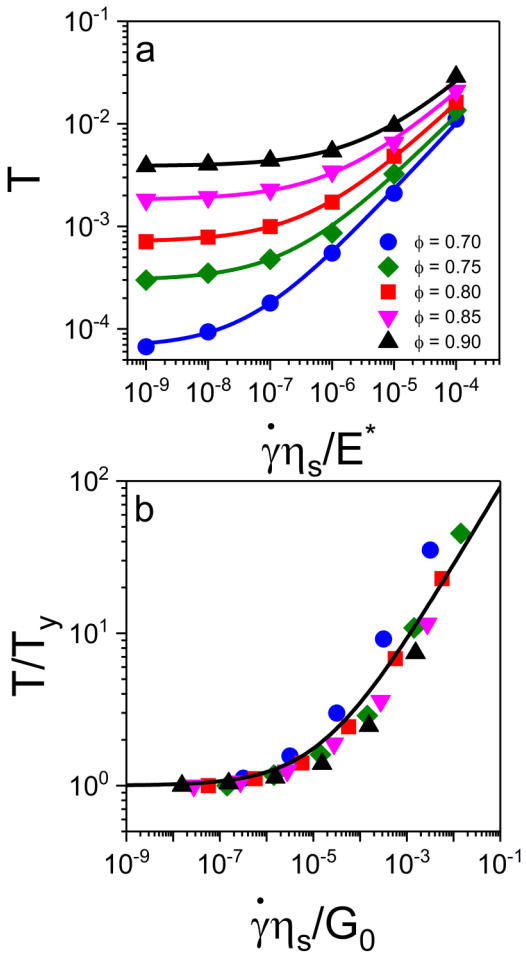

FIG. 5. (a) Temperature T as a function of the shear rate $\dot{\gamma}\eta_s/E^*$ and (b) master curve of the rescaled temperature T/T_y as a function of the rescaled shear rate $\dot{\gamma}\eta_s/G_0$ for SPGs with different volume fractions. The solid lines in (a) show the HB equation fit to data given by $T = T_y + k(\eta_s\dot{\gamma}/E^*)^n$. The solid line in (b) shows the HB equation fit to data given by $T/T_y = 1 + 301(\eta_S\dot{\gamma}/G_0)^{0.52}$.

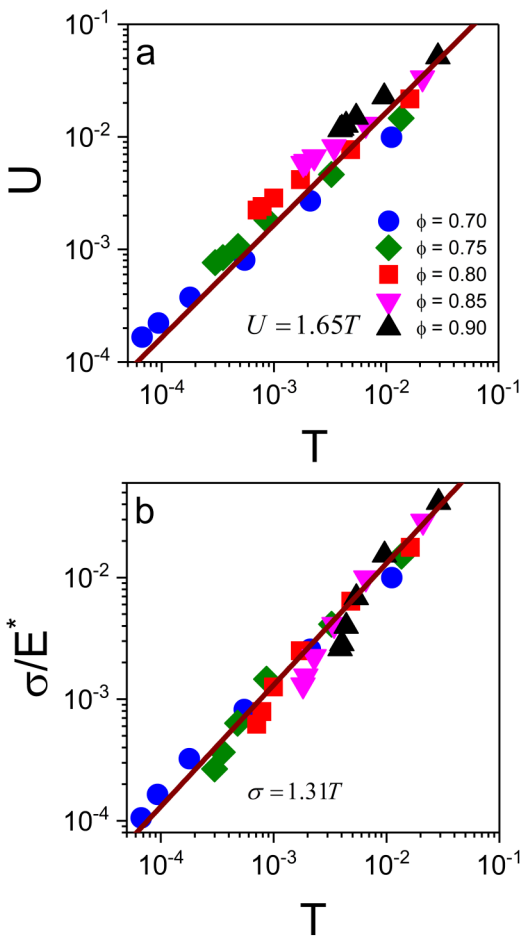

FIG. 6. (a) Elastic energy U and (b) shear stress σ/E^* as a function of temperature T for SPGs with different volume fractions. The solid lines are the linear fit to data.

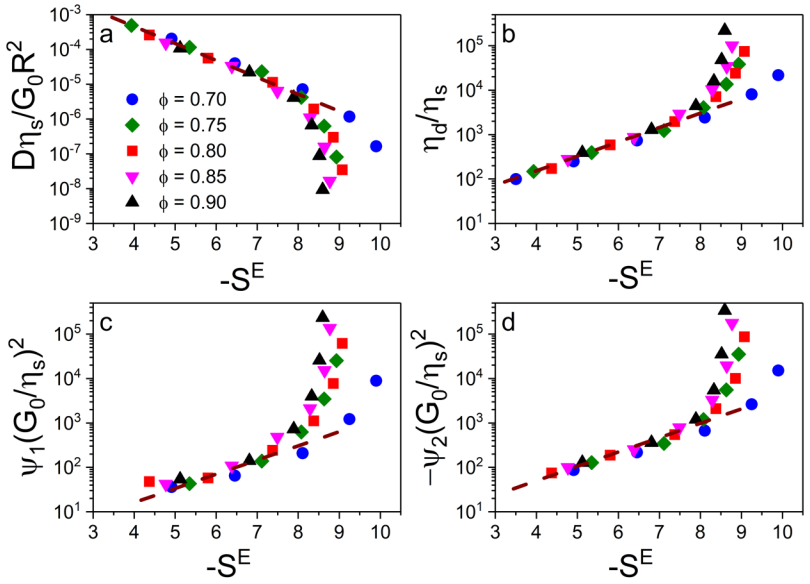

FIG. 7. Master curve of (a) diffusion coefficient $D\eta_s/G_0R^2$, (b) shear viscosity, (c) first, and (d) second normal stress coefficient as a function of the $-S^E$. The dashed lines show the linear fits to data at large values of S^E.

entropy of the SPGs. A universal exponential correlation between the diffusion coefficient and the excess entropy, i.e., $D\eta_s/R^2G_0 \sim \exp(\alpha S^E)$ is observed at low values of $-S^E$ with $\alpha \cong 1.1$, slightly higher than the value of 1.0 that is typically seen. At low shear rate and excess entropy, which corresponds to the quasistatic regime, the diffusion coefficient exhibits a sharp downward turn due to the solidlike nature of SPGs in this regime.

The rheology of SPGs is also correlated with the excess entropy by determining three viscometric functions, namely, the shear viscosity and the first and second normal stress coefficients. The shear viscosity is defined as the ratio of yielding part of the shear stress to the shear rate as $\eta_d = (\sigma - \sigma_y)/\dot{\gamma}$, and the first and second normal stress differences are defined as $\psi_1 = N_1/\dot{\gamma}^2$ and $\psi_2 = N_2/\dot{\gamma}^2$, respectively. The rescaled shear viscosity with respect to the solvent viscosity η_d/η_s is plotted as a function of $-S^E$ in Fig. 7(b). The shear viscosity increases with a decrease in the excess entropy. At large S^E, the shear viscosity decreases (shear thinning behavior) and shows an exponential decay with respect to S^E as $\eta_d \sim \eta_s \exp(-\beta S^E)$, where $\beta = \alpha \cong 1.1$. At smaller excess entropy that corresponds to yield behavior, the viscosity significantly increases and deviates from the exponential variation at high shear rates The first and second normal stress coefficients show the same behavior as a function of the S^E. Note that the transition from the quasistatic regime to the shear thinning occurs at the same excess entropy (close to $-S^E \cong 9$) or equivalently the same shear rate in all of the macroscopic properties.

IV. DISCUSSION

The shear-induced diffusivity, dynamic viscosity, and normal stress coefficients for different volume fractions and shear rates collapse onto master curves of the excess entropy. However, the excess entropy thus far has been determined from detailed measurements of the microstructure, which are not often convenient or easily accessible. The expression of the excess entropy in terms of other more easily measurable quantities through an equation of state would be useful.

An equation of state relating the easily measurable shear stress to the excess entropy can be constructed from the observations in Fig. 6 that the energy and shear stress are linearly proportional to the temperature according to $U = 1.65T$ and $\sigma = 1.31T$. From this and $(dU/dS^E)_{N,V} = T$, we find that $1.65(d\sigma/dS^E)_{N,V} = \sigma$, which after integration becomes the equation of state,

$$-S^E = -S_y^E - B \ln\frac{\sigma}{\sigma_y}, \tag{7}$$

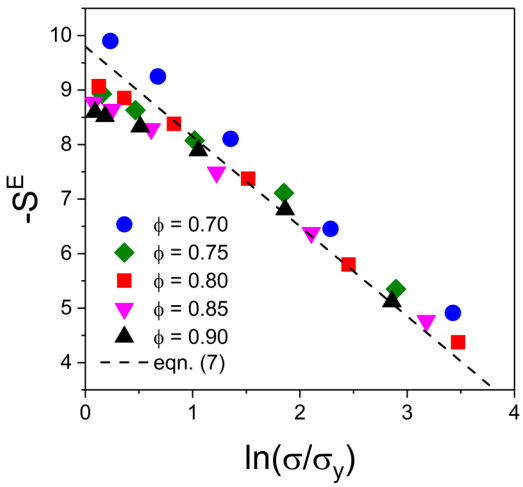

FIG. 8. Master curve of the excess entropy $-S^E$ as a function of the shear stress $\ln(\sigma/\sigma_y)$. The best fit using Eq. (7) to data is shown by the dashed line.

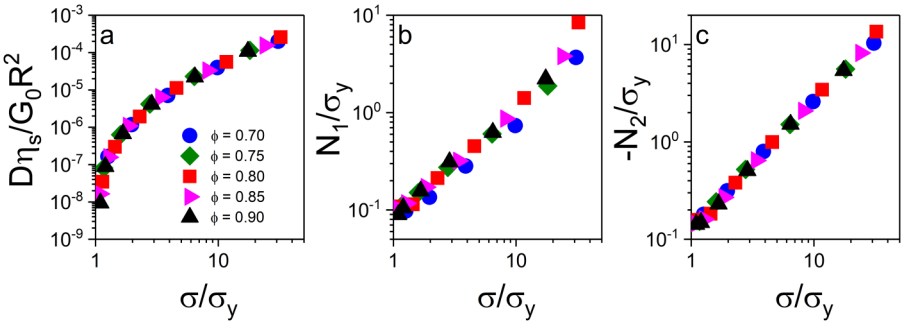

FIG. 9. (a) Diffusion coefficient $D\eta_s/R^2G_0$, (b) first normal stress difference $\Psi_1(G_0/\eta_s)^2$, and (c) second normal stress difference $-\Psi_2(G_0/\eta_s)^2$ as a function of shear stress σ/σ_y obtained for SPGs with different volume fractions.

where B is a constant and $-S_y^E$ is the excess entropy at the yield point. Thus, the excess entropy can be determined from the shear stress flow curve. Indeed the shear stress follows the prediction of Eq. (7) as shown in Fig. 8. Based on the fit to data $-S_y^E$ is 9.8 ± 0.07 and B is 1.35 ± 0.09, which is close to 1.65 ± 0.10 that can be obtained from the relationships among U, σ, and T. We should note that the linear fits in Fig. 6 are not perfect given that it covers almost three orders of magnitude of the data, but this form had the highest R^2 values of many tested. Considering these uncertainties, the value of B is consistent.

Figure 7 shows that the diffusivity and normal stress coefficients follow the excess entropy scaling. Thus, from Eq. (7), we can expect these dynamical properties to fall onto a master curve of the shear stress normalized by the yield stress. In Fig. 9(a), the diffusion coefficient $D\eta_s/R^2G_0$ is plotted as a function of the shear stress σ/σ_y. The diffusion coefficients of SPGs increase with the applied shear stress and show a universal behavior. Furthermore, the first and second normal stress coefficients, $\Psi_1(G_0/\eta_s)^2$ and $-\Psi_2(G_0/\eta_s)^2$, plotted against the shear stress in Figs. 9(b) and 9(c) also show the collapse onto a master curve. Thus, from the measurement of the shear stress flow curve, the shear diffusivity and the two normal stresses can be determined. Remarkably, the measurement of any one of the four dynamical properties (i.e., diffusivity, shear stress or viscosity, and first and second normal stress coefficients) allows one to determine the other three.

This interrelationship among the transport coefficients was also found by relating them to the microstructural relaxation time for the SPG [22]. This is the time required for a particle to escape a cage of surrounding particles when the suspension is sheared. Indeed, the microstructural relaxation time for SPGs at different concentrations and shear rates versus the excess entropy all collapse onto a single master curve (see Fig. S2 in supplementary material [37]). Similar results for microstructural relaxation times have been observed for equilibrium [8] and sheared Brownian suspensions [24].

In order to compare the results of current simulations of SPGs with other systems, such as monodispersed and bidispersed suspensions of hard spheres, metallic glasses, and Gaussian core fluids [1,7,9–11,13,19], the generalized diffusion coefficient D^*, which was proposed by Dzugutov [2], is determined as follows:

$$D^* = \frac{D_i}{\chi_i}, \tag{8}$$

where χ_i is the scaling factor, which is defined as

$$\chi_i = 4(\pi k_B T)^{1/2} \sum_{j=1}^{N_c} x_i \rho \sigma_{ij}^4 g_{ij}(\sigma_{ij}) \left(\frac{m_i + m_j}{m_i m_j}\right)^{1/2}, \tag{9}$$

and k_B is the Boltzmann constant, x_i is the mole fraction of component i, $g_{ij}(\sigma_{ij})$ is the magnitude of the pair distribution function between particles i and j determined at the contact, and m_i is the mass of particle i. Note that in our case, the system of interest is a single component; thus, $\chi = R^2G_0/\eta_s$. The generalized diffusion coefficient D^* for monodisperse and bidisperse hard spheres, liquid metals, and SPGs are plotted against $-S^E$ for various systems in Fig. 10. There appears a master curve that includes both the athermal and equilibrium systems. This means that measurements or predictions of diffusivity from an equilibrium system can be

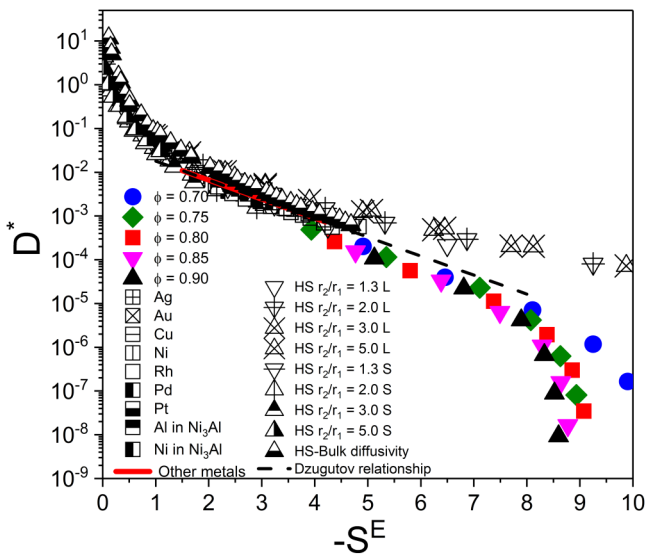

FIG. 10. The generalized diffusion coefficient D^* obtained in current simulations of SPGs (filled symbols), metals [square and red line (in color on line) and black (in print)] [7,11], and hard spheres (open and half-filled triangles) [10,18], as a function of $-S^E$ for different systems.

used to predict those in an athermal nonequilibrium system at the same excess entropy and vice versa, provided that both follow the excess entropy scaling. Similar results are expected for viscosity and other transport properties.

The master curve for diffusivity breaks down for bidisperse hard spheres at moderate to low values of the excess entropy. The deviation occurs even before the diffusivity of the SPGs drops dramatically. The deviation may, in part, be due to the choice of the scaling for diffusivity. The collapse of data for molecular systems has been found to be sensitive to the choice of scaling [16], and this may explain the deviation seen with the bidisperse hard spheres.

V. CONCLUSIONS

We have shown that the shear-induced diffusivity, dynamic viscosity, and first and second normal stress coefficients obey an excess entropy scaling. To the best of our knowledge, this is the first time such a scaling has been demonstrated for a system that is shear activated with negligible thermal forces. At moderate values of the excess entropy, the normalized diffusivity and viscosity scale like $e^{\alpha S^E}$ and $e^{-\alpha S^E}$, as observed originally by Rosenfeld, Dzugutov, and others. At larger values of the excess entropy, near the yielding of the stress of the SPGs, the diffusivity approaches zero and the viscosity and normal stress coefficients approach infinity as $-S^E$ approaches a finite value. Interestingly, suitably normalized diffusivities from a variety of equilibrium thermal and the athermal sheared SPG system presented here collapse on a universal curve for excess entropy. This provides an intriguing connection between equilibrium and nonequilibrium and a possible means to predict properties of one from the other.

An effective temperature can also be derived for this sheared system from the computed relationship between elastic energy and excess entropy. For the SPGs, the temperature scales linearly with both the shear stress and elastic energy. An equation of state can then be derived to predict the excess entropy from measurements of shear stress. This equation of state then allows one to predict any transport property (e.g., shear-induced diffusivity or normal stresses) from the measurement of another (e.g., the shear stress).

ACKNOWLEDGMENTS

F.K. and R.T.B. gratefully acknowledge partial financial support from the National Science Foundation (NSF) (MRSEC under Award No. DMR-1720595).

REFERENCES

[1] Rosenfeld, Y., "Relation between the transport coefficients and the internal entropy of simple systems," Phys. Rev. A **15**(6), 2545 (1977).
[2] Dzugutov, M., "A universal scaling law for atomic diffusion in condensed matter," Nature **381**(6578), 137–139 (1996).
[3] Baranyai, A., and D. J. Evans, "Direct entropy calculation from computer simulation of liquids," Phys. Rev. A **40**(7), 3817 (1989).
[4] Dyre, J. C., "Perspective: Excess-entropy scaling," J. Chem. Phys. **149**(21), 210901 (2018).
[5] Grover, R., W. G. Hoover, and B. Moran, "Corresponding states for thermal conductivities via nonequilibrium molecular dynamics," J. Chem. Phys. **83**(3), 1255–1259 (1985).
[6] Guan, P., M. Chen, and T. Egami, "Stress-temperature scaling for steady-state flow in metallic glasses," Phys. Rev. Lett. **104**(20), 205701 (2010).
[7] Hoyt, J., M. Asta, and B. Sadigh, "Test of the universal scaling law for the diffusion coefficient in liquid metals," Phys. Rev. Lett. **85**(3), 594 (2000).
[8] Ingebrigtsen, T. S., J. R. Errington, T. M. Truskett, and J. C. Dyre, "Predicting how nanoconfinement changes the relaxation time of a supercooled liquid," Phys. Rev. Lett. **111**(23), 235901 (2013).
[9] Krekelberg, W. P., T. Kumar, J. Mittal, J. R. Errington, and T. M. Truskett, "Anomalous structure and dynamics of the Gaussian-core fluid," Phys. Rev. E **79**(3), 031203 (2009).
[10] Krekelberg, W. P., M. J. Pond, G. Goel, V. K. Shen, J. R. Errington, and T. M. Truskett, "Generalized Rosenfeld scalings for tracer diffusivities in not-so-simple fluids: Mixtures and soft particles," Phys. Rev. E **80**(6), 061205 (2009).
[11] Li, G., C. Liu, and Z. Zhu, "Excess entropy scaling for transport coefficients: Diffusion and viscosity in liquid metals," J. Non-Cryst. Solids **351**(10–11), 946–950 (2005).
[12] Rosenfeld, Y., "Excess-entropy and freezing-temperature scalings for transport coefficients: Self-diffusion in Yukawa systems," Phys. Rev. E **62**(5), 7524–7527 (2000).
[13] Vaz, R. V., A. L. Magalhães, D. L. A. Fernandes, and C. M. Silva, "Universal correlation of self-diffusion coefficients of model and real fluids based on residual entropy scaling law," Chem. Eng. Sci. **79**, 153–162 (2012).
[14] Rosenfeld, Y., "A quasi-universal scaling law for atomic transport in simple fluids," J. Phys. Condens. Matter **11**(28), 5415–5427 (1999).
[15] Lötgering-Lin, O., M. Fischer, M. Hopp, and J. Gross, "Pure substance and mixture viscosities based on entropy scaling and an analytic equation of state," Ind. Eng. Chem. Res. **57**(11), 4095–4114 (2018).
[16] Hopp, M., J. Mele, and J. Gross, "Self-diffusion coefficients from entropy scaling using the PCP-SAFT equation of state," Ind. Eng. Chem. Res. **57**(38), 12942–12950 (2018).
[17] Ma, X., J. Liu, Y. Zhang, P. Habdas, and A. G. Yodh, "Excess entropy and long-time diffusion in colloidal fluids with short-range interparticle attraction," J. Chem. Phys. **150**(14), 144907 (2019).
[18] Mittal, J., J. R. Errington, and T. M. Truskett, "Thermodynamics predicts how confinement modifies the dynamics of the equilibrium hard-sphere fluid," Phys. Rev. Lett. **96**(17), 177804 (2006).
[19] Fomin, Y. D., V. Ryzhov, and N. Gribova, "Breakdown of excess entropy scaling for systems with thermodynamic anomalies," Phys. Rev. E **81**(6), 061201 (2010).
[20] Seth, J. R., L. Mohan, C. Locatelli-Champagne, M. Cloitre, and R. T. Bonnecaze, "A micromechanical model to predict the flow of soft particle glasses," Nat. Mater. **10**(11), 838–843 (2011).
[21] Khabaz, F., T. Liu, M. Cloitre, and R. T. Bonnecaze, "Shear-induced ordering and crystallization of jammed suspensions of soft particles glasses," Phys. Rev. Fluids **2**(9), 093301 (2017).
[22] Khabaz, F., M. Cloitre, and R. T. Bonnecaze, "Particle dynamics predicts shear rheology of soft particle glasses," J. Rheol. **64**(2), 1–10 (2020).
[23] Krekelberg, W. P., V. Ganesan, and T. M. Truskett, "Shear-rate-dependent structural order and viscosity of a fluid with short-range attractions," Phys. Rev. E **78**(1), 010201 (2008).
[24] Ingebrigtsen, T. S., and H. Tanaka, "Structural predictor for nonlinear sheared dynamics in simple glass-forming liquids," Proc. Natl. Acad. Sci. U.S.A. **115**(1), 87–92 (2018).
[25] Ding, Y., and J. Mittal, "Equilibrium and nonequilibrium dynamics of soft sphere fluids," Soft Matter **11**(26), 5274–5281 (2015).

[26] Liu, T., F. Khabaz, R. T. Bonnecaze, and M. Cloitre, "On the universality of the flow properties of soft-particle glasses," Soft Matter **14**(34), 7064–7074 (2018).

[27] Khabaz, F., M. Cloitre, and R. T. Bonnecaze, "Structural state diagram of concentrated suspensions of jammed soft particles in oscillatory shear flow," Phys. Rev. Fluids **3**(3), 033301 (2018).

[28] Mohan, L., C. Pellet, M. Cloitre, and R. Bonnecaze, "Local mobility and microstructure in periodically sheared soft particle glasses and their connection to macroscopic rheology," J. Rheol. **57**(3), 1023–1046 (2013).

[29] Liu, K. K., D. R. Williams, and B. J. Briscoe, "The large deformation of a single micro-elastomeric sphere," J. Phys. D Appl. Phys. **31**(3), 294–303 (1998).

[30] Lees, A. W., and S. F. Edwards, "The computer study of transport processes under extreme conditions," J. Phys. C Solid State Phys. **5**(15), 1921–1928 (1972).

[31] Plimpton, S., "Fast parallel algorithms for short-range molecular dynamics," J. Comput. Phys. **117**(1), 1–19 (1995).

[32] Larson, R. G., *The Structure and Rheology of Complex Fluids* (Oxford University, New York, 1999).

[33] Seth, J. R., M. Cloitre, and R. T. Bonnecaze, "Elastic properties of soft particle pastes," J. Rheol. **50**(3), 353–376 (2006).

[34] Cloitre, M., R. Borrega, F. Monti, and L. Leibler, "Glassy dynamics and flow properties of soft colloidal pastes," Phys. Rev. Lett. **90**(6), 068303 (2003).

[35] Dzugutov, M., "Dynamical diagnostics of ergodicity breaking in supercooled liquids," J. Phys. Condens. Matter **11**(10A), A253–A259 (1999).

[36] Mohan, L., and R. T. Bonnecaze, "Short-ranged pair distribution function for concentrated suspensions of soft particles," Soft Matter **8**(15), 4216–4222 (2012).

[37] See the supplementary material at https://doi.org/10.1122/1.5133852 for supporting information discussed in the main text.